

Eigenanalysis-Based Space-Time Adaptive Radar: Performance Analysis

A. M. HAIMOVICH

M. BERIN

New Jersey Institute of Technology

The space-time radar problem is well suited to the application of techniques that take advantage of the low rank property of the space-time covariance matrix. The performance of an eigenanalysis-based detector with respect to convergence rate and robustness to calibration errors is analyzed. Analytical expressions are developed for receiver operating curves when the clutter signal environment is assumed to be Gaussian. The curves are derived from the asymptotic expansion of the distribution of the principal components of the covariance matrix. Simulation results are provided to corroborate the theoretical analysis. Examples from the Mountain-Top dataset are used to illustrate the higher convergence rate and increased robustness of the eigenanalysis method.

Manuscript received August 1, 1995; revised September 3, 1996.

IEEE Log No. T-AES/33/4/06841.

Authors' current addresses: A. M. Haimovich, New Jersey Institute of Technology, Electrical and Computer Engineering Dept., University Heights, Newark, NJ 07102; M. Berin, Expert Wireless Solutions, Inc., Fort Lee, NJ.

0018-9251/97/\$10.00 © 1997 IEEE

I. INTRODUCTION

Airborne surveillance radars are faced with the difficult task of detecting weak moving targets in strong clutter and interference environments. Typically, the spatial and temporal spectra of the clutter is unknown and varying, hence adaptive techniques with fast convergence rate are important to the designers of next generation air surveillance radars. The airborne radar problem is two-dimensional, with echoes of a moving target being a function of both angle and frequency. A *space-time* receiver architecture that consists of an antenna array and provides temporal filtering of each spatial channel is capable of exploiting the information in both domains.

The theory of space-time adaptive processing (STAP) was pioneered by Brennan and Reed [1]. They showed that the optimal Neyman-Pearson detector for a known signal vector in colored Gaussian noise with a known covariance matrix is linear, i.e., it consists of a linear combination of the components of the vector. In practice, the noise (a collective reference to background noise + clutter + jammers) covariance matrix is typically not known. The common approach is to estimate it from a *secondary* data set that does not contain the signal of interest. In radar, the secondary data may be composed of signals from range cells adjacent to the one under observation. Reed, et al. suggested the Sample Matrix Inversion (SMI) method, in which an estimate is substituted for the noise covariance matrix expression in the linear detector [2]. They developed an expression for the density of the signal-to-noise ratio (SNR) loss with respect to the optimal case and showed that if the signal vector dimension is N , the number of samples required to achieve performance with 3 dB of the optimal, is approximately $K = 2N$. This convergence has the remarkable property of being independent from the true noise covariance matrix. Other authors have analyzed the performance of the linear detector with estimated covariance matrix [3–5]. While preserving the linear architecture of the detector, the SMI detector has a number of drawbacks: 1) it is not optimal for detection performance, 2) it has slow convergence for large N , 3) it is sensitive to calibration errors, and 4) it is not constant false-alarm rate (CFAR). Subsequent work addressed some of these concerns. A detector for a signal vector with unknown amplitude and in unknown colored noise was derived by Kelly from a generalized likelihood ratio (GLR) test [6]. Unfortunately, the GLR-based detector is more complex and has convergence properties similar to the SMI detector. The SMI method was shown to be sensitive to calibration errors [7, 8]. Various remedies have been suggested, for example, [9, 10], which reduce sensitivity to calibration errors at the expense of some added

complexity. CFAR modifications of the SMI detector were suggested and analyzed in [11 and 12]. While deficiencies of the SMI detector have been addressed on an individual basis, a comprehensive approach for the design of a linear detector with fast convergence, increased robustness, and CFAR capability, has been lacking. We advance that most of these desired features can be achieved in the case of STAP radar, by a linear eigenanalysis-based detector. Such a detector is derived from partitioning the signal space into *interference* and *noise* subspaces and computing a weight vector in the noise subspace. The interference subspace contains the clutter contributions. Two forms of the eigenanalysis-based detector have been referred to as the eigencanceler [13, 14] and the PCI method in [15]. The eigencanceler is a modification of the minimum variance beamformer. The minimum variance beamformer minimizes the array output subject to a set of linear constraints [16]. The eigencanceler produces the minimum norm weight vector meeting the set of linear constraints, and subject to the additional constraint of orthogonality to the interference subspace [17]. The PCI is derived as a linear detector of data from which the interference has been removed [15]. In the case of a single steering vector constraint, the two methods provide similar solutions. In [14] we show that the space-time clutter covariance matrix for a uniform array and fixed pulse-repetition frequency (PRF) is essentially low rank, due to the inherent oversampling nature of the STAP architecture. Hence, the space-time radar problem is well suited to the application of techniques that take advantage of the low-rank property. The eigenanalysis-based method has been shown to have a faster convergence rate than the SMI method. Specifically, it has been shown that the number of samples required for an average loss of 3 dB with respect to the optimal detector is $2r$, where r is the interference space rank [18, 19]. This finding is particularly significant when $r \ll N$, which turns out to be the case for a typical space-time radar. This work analyzes the performance of the eigenanalysis-based detector with respect to convergence rate and sensitivity to calibration errors. Theoretical probability of detection expressions derived analytically are corroborated by simulations. Convergence rate and robustness are analyzed and compared with the SMI method. The analysis and numerical results clearly indicate the advantages of the eigenanalysis approach for space-time radar. These results are further supported by processing and analysis of Mountain-Top dataset.

This work is organized as follows. Section II introduces the signal model, Section III provides the performance analysis with respect to detection and calibration errors, and it presents simulations numerical results. The Mountain-Top data is analyzed

in Section IV. Section V provides the summary and conclusions.

II. SIGNAL MODEL

Consider a space-time array with ν antennas uniformly spaced and a κ -pulse coherent pulse interval (CPI). The array is sidelooking, i.e., its axis is parallel to the flight axis. The complex envelope of the signal received at the array from a point source is given by the vector $\mathbf{s}_s = (1, \dots, e^{j(\nu-1)u})^T$, where u is the normalized spatial frequency given by

$$u = \frac{2\pi}{\lambda} d \sin \theta \quad (1)$$

and d , λ , and θ are the interelement spacing, wavelength, and angle of arrival, respectively. The complex envelope sampled at the first array element is represented by the vector $\mathbf{s}_t = (1, \dots, e^{j(\nu-1)v})^T$, where v is the normalized Doppler frequency

$$v = \frac{2v_r}{\lambda f_r} \quad (2)$$

and v_r and f_r are the radar-target radial velocity and the radar PRF, respectively. The $(N = \nu\kappa)$ -dimensional target vector is defined

$$\mathbf{s} = \frac{1}{\sqrt{N}} \mathbf{s}_s \otimes \mathbf{s}_t \quad (3)$$

where \otimes denotes the Kronecker product. Under hypothesis \mathbf{H}_0 the received signal \mathbf{x} consists only of clutter \mathbf{c} and noise \mathbf{v} contributions:

$$\mathbf{x} = \mathbf{c} + \mathbf{v} \quad (4)$$

where \mathbf{x} is assumed a zero-mean, circularly symmetric complex Gaussian random vector with covariance matrix \mathbf{R} . Under hypothesis \mathbf{H}_1 , \mathbf{x} is given by

$$\mathbf{x} = a\mathbf{s} + \mathbf{c} + \mathbf{v} \quad (5)$$

where a is a zero-mean, circularly symmetric complex Gaussian random variable with variance σ_s^2 .

Since the colored noise (colored noise refers to the aggregate of noise + clutter + interferences) covariance matrix is usually not known, an estimate is used. The estimate is derived from range cells in the vicinity of the tested range cell (referred to as "secondary data"). The secondary data consists of clutter returns and, possibly, other interferences, such as jammers. The presence of narrowband jammers does not alter the signal model as presented, thus we restrict our attention only to clutter signals. Wideband jammers are not considered here. In the sequel, the terms clutter and interference are used interchangeably. The assumption is that the secondary \mathbf{x}_k , $k = 1, \dots, K$, data has the same statistical properties as the tested cell under hypothesis model \mathbf{H}_0 . The maximum likelihood estimate of the covariance matrix is given by

$$\hat{\mathbf{R}} = \frac{1}{K} \sum_{k=1}^K \mathbf{x}_k \mathbf{x}_k^H \quad (6)$$

The SMI weight vector is given by the well-known relation

$$\mathbf{w} = k\hat{\mathbf{R}}^{-1}\mathbf{s} \quad (7)$$

where k is a gain constant.

It has been shown that the space-time covariance matrix of the secondary data of a well-calibrated, uniform array employing a fixed PRF, can be decomposed into low rank interference, representing the clutter, and white noise contributions [14]. Its spectral decomposition can be written

$$\mathbf{R} = \mathbf{Q}_c\mathbf{\Lambda}_c\mathbf{Q}_c^H + \sigma_v^2\mathbf{Q}_v\mathbf{Q}_v^H \quad (8)$$

where the diagonal of the $r \times r$ matrix $\mathbf{\Lambda}_c$ consists of the r principal eigenvalues of \mathbf{R} , the columns of \mathbf{Q}_c are the corresponding eigenvectors, σ_v^2 is the variance of the white noise, and the columns of \mathbf{Q}_v are the remaining eigenvectors of \mathbf{R} . The subspaces spanned by the columns of \mathbf{Q}_c and \mathbf{Q}_v are referred to as *interference* and *noise*, respectively. The interference subspace represents the clutter returns. Under a set of special conditions,¹ the rank of the interference subspace is upper bounded by $r_{\max} = \nu + \kappa - 1$. The low rank property has been found empirically in [20] and is explained in [14]. The actual covariance matrix derived from observed data will not exhibit equal noise eigenvalues. Nevertheless, in a high clutter environment, the matrix will be approximately low rank, as illustrated in Fig. 1. This figure shows the eigenvalue distribution of data extracted from the Mountain-Top dataset. The Mountain-Top data collection has been characterized in [21]. It consists of a mountain-top installation that emulates an airborne pulse Doppler radar through coherent sequential transmissions from the antennas of the array. The antenna array consists of 14 elements, and the CPI has 16 pulses, hence the dimension of the space-time covariance matrix is 224 resulting in the same number of eigenvalues shown on the abscissa of Fig. 1. The ordinate represents the ratio in dB of the eigenvalues magnitude to the average noise power. The noise power was computed from a separate file supplied with the data. While $r_{\max} = 14 + 16 - 1 = 29$, the actual number of principal eigenvalues (eigenvalues significantly larger than the rest) is seen to be only about 6. This is due to the fact that the clutter cover blankets only a portion of the space-time domain. The horizontal line through 0 dB represents the average noise power. The low rank property of the space-time covariance matrix is evident in the figure and motivates the pursuit of eigenanalysis-based techniques.

The eigencanceler was formulated in [17] as a modified minimum variance beamformer. It processes

¹The conditions necessary for the rule $r_{\max} = \nu + \kappa - 1$ to hold are: linear equispaced array with $d/\lambda \leq 0.5$ (spatial Nyquist), $\text{PRF} \geq$ clutter bandwidth (temporal Nyquist), no crab angle, no channel errors, no channel fluctuations, zero system bandwidth.

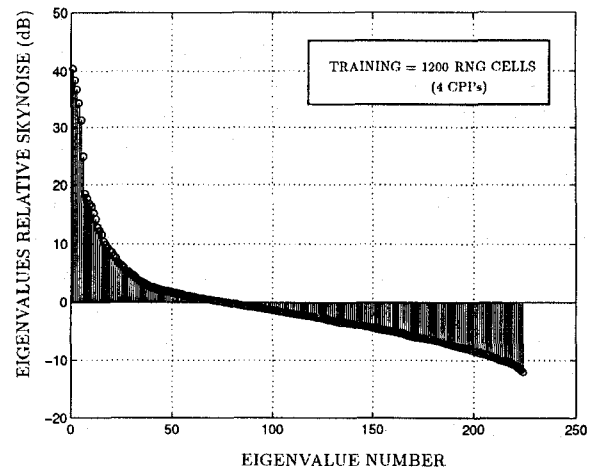


Fig. 1. Eigenvalues of space-time covariance matrix.

the data with the following weight vector:

$$\begin{aligned} \mathbf{w} &= (\mathbf{I}_N - \mathbf{Q}_c\mathbf{Q}_c^H)\mathbf{g} \\ &= \mathbf{Q}_v\mathbf{Q}_v^H\mathbf{g} \end{aligned} \quad (9)$$

where $\mathbf{g} = [\mathbf{C}^H(\mathbf{I}_N - \mathbf{Q}_c\mathbf{Q}_c^H)\mathbf{C}]^{-1}\mathbf{f}$, and $\mathbf{C}^H\mathbf{w} = \mathbf{f}$ is a set of linear constraints. The columns of the matrix \mathbf{Q}_c consist of the principal eigenvectors of the clutter covariance matrix. Note that the eigencanceler substitutes the noise subspace for the inverse covariance matrix in the minimum variance beamformer. For the case when the single gain constraint is $\mathbf{s}^H\mathbf{w} = \text{constant}$, the weight vector is given, within a scaling factor, by $\mathbf{w} = (\mathbf{I}_N - \mathbf{Q}_c\mathbf{Q}_c^H)\mathbf{s}$. When the covariance matrix is estimated from the secondary data, the interference subspace \mathbf{Q}_c in (9), is substituted with the estimated subspace $\hat{\mathbf{Q}}_c$.

III. PERFORMANCE ANALYSIS

This section provides the performance analysis for the eigenanalysis-based method with respect to detection and robustness to calibration errors. Results are interpreted through a performance comparison with the SMI method.

A. Detection

A widely accepted measure of performance for radar systems is the probability of detection curves. These curves show the probability of detection with the input SNR as an independent variable and the probability of false alarm as a parameter. In adaptive radar, detection probability is a function of the weight vectors. In turn, weight vectors are derived from estimates of the covariance matrix of the secondary data, and as such are random variables. This makes the detection probability realization-dependent. To assess the receiver operation under a wide variety of conditions, it is desired to generate average probability

of detection curves. A convenient procedure consists of expressing the detection probability as a function of the *conditioned SNR*. The conditioned SNR is defined as the effective normalized by the optimal SNR:

$$\rho = \frac{\text{SNR}_{\text{eff}}}{\text{SNR}_{\text{opt}}} = \frac{|\mathbf{w}^H \mathbf{s}|^2}{\mathbf{w}^H \mathbf{R} \mathbf{w}} \frac{1}{\mathbf{s}^H \mathbf{R}^{-1} \mathbf{s}} \quad (10)$$

where SNR_{eff} is defined as the ratio between the target power and the colored noise power at the array output, i.e.,

$$\text{SNR}_{\text{eff}} = \frac{|\mathbf{w}^H \mathbf{s}|^2}{\mathbf{w}^H \mathbf{R} \mathbf{w}} \quad (11)$$

and $\text{SNR}_{\text{opt}} = \mathbf{s}^H \mathbf{R}^{-1} \mathbf{s}$. The conditioned SNR is a random variable, always bounded $0 \leq \rho \leq 1$. The density of the conditioned SNR for the SMI method with Gaussian data has been characterized in [2]:

$$f(\rho) = \text{const} \times (1 - \rho)^{N-2} \rho^{K+1-N}, \quad 0 \leq \rho \leq 1. \quad (12)$$

The density of the conditioned SNR for the eigenanalysis-based detector has been derived in [19]. The development is based on the asymptotic expansion of the distribution of the principal components of the covariance matrix. Therein it is shown that the conditioned SNR can be expressed as

$$\rho = \frac{1}{1 + \frac{1}{K} \zeta} \quad (13)$$

where $\zeta = \sum_{i=1}^r \nu_i$, and ν_i are independent identically distributed (IID) random variables with exponential distribution and hence, ζ is a Gamma random variable with r degrees of freedom and parameter 1. This characterization results in the density

$$f(\rho) = K \rho^{-2} \sum_{i=1}^r \frac{\pi_i}{\bar{\nu}_i} \exp\left(\frac{-K \left(\frac{1}{\rho} - 1\right)}{\bar{\nu}_i}\right) \quad (14)$$

where $\pi_i = \prod_{j=1, j \neq i}^r \bar{\nu}_j / (\bar{\nu}_j - \bar{\nu}_i)$. The usefulness of this expression has been demonstrated by Monte Carlo simulations presented in the reference. Also shown in the reference is that for large clutter-to-noise ratio (CNR) and large K ($K \geq 10$),

$$\rho \cong 1 - \frac{1}{K} \zeta. \quad (15)$$

From (15), and using the property of the gamma distribution, $E[\zeta] = r$, the condition $E[\rho] = 1/2$ is met for $K = 2r$. This property is significant in the space-time array since $r = \nu + \kappa - 1 \ll \nu \kappa = N$ holds even for moderate size arrays. A higher convergence rate is tantamount to achieving the same performance level using estimates based on smaller secondary datasets. Since the clutter environment can be assumed only locally homogeneous, an increased convergence

rate could be essential to the proper operation of the system.

The decision statistic for detection conditioned on the weight vector is given by the instantaneous output power:

$$\eta = |\mathbf{w}^H \mathbf{x}|^2. \quad (16)$$

When \mathbf{x} is the signal received from the cell under test and is modeled as a complex Gaussian random vector with circular symmetry under both hypothesis models, the statistic η has an exponential density:

$$f_\eta(\eta | H_i, \mathbf{w}) = \frac{1}{\bar{\eta}_i} e^{-\eta/\bar{\eta}_i} \quad (17)$$

where $i = 1, 2$, and the statistic mean values are $\bar{\eta}_1 = E_{H_1}[\eta] = \sigma_s^2 |\mathbf{w}^H \mathbf{s}|^2 + \mathbf{w}^H \mathbf{R} \mathbf{w}$ and $\bar{\eta}_0 = E_{H_0}[\eta] = \mathbf{w}^H \mathbf{R} \mathbf{w}$. Scaling of the weight vector does not affect the conditioned SNR. To simplify notation, it is assumed that the gain of \mathbf{w} has been set such that $\mathbf{w}^H \mathbf{s} = 1$. For a given threshold η_T , the probability of detection is given by

$$P_d = \int_{\eta_T}^{\infty} f_\eta(\eta | H_1, \mathbf{w}) d\eta = e^{-\eta_T/\bar{\eta}_1}. \quad (18)$$

The probability of false alarm is given by

$$P_f = \int_{\eta_T}^{\infty} f_\eta(\eta | H_0, \mathbf{w}) d\eta = e^{-\eta_T/\bar{\eta}_0}. \quad (19)$$

The mean value of the decision statistic is equal to the average output power. An upper bound on the performance can be obtained from the case when the true noise covariance matrix is known. Then, the optimal weight vector with the unit signal gain constraint is given by $\mathbf{w} = k \mathbf{R}^{-1} \mathbf{s}$, with $k = (\mathbf{s}^H \mathbf{R}^{-1} \mathbf{s})^{-1}$. The output power under H_0 is given by

$$\bar{\eta}_0 = \frac{1}{\mathbf{s}^H \mathbf{R}^{-1} \mathbf{s}} = k \equiv \frac{1}{\alpha}. \quad (20)$$

From which the probability of false alarm is

$$P_f = e^{-\alpha \eta_T}. \quad (21)$$

The probability of detection can be expressed directly in terms of the probability of false alarm by noting that the output power under H_1 is

$$\bar{\eta}_1 = \sigma_s^2 + \frac{1}{\mathbf{s}^H \mathbf{R}^{-1} \mathbf{s}} = \sigma_s^2 + \frac{1}{\alpha} \quad (22)$$

from which it follows that the probability of detection, expressed as a function of the probability of false alarm, is

$$P_d = e^{-\eta_T/\bar{\eta}_1} = P_f^{1/(1+\alpha\sigma_s^2)}. \quad (23)$$

To obtain expressions for the detection probability of the SMI and the eigenanalysis methods, we observe

that, under either hypothesis, the output power can be expressed in terms of the conditioned SNR ρ and the parameter α . From (10) and (16) the conditional output power under \mathbf{H}_0 is

$$\bar{\eta}_0 = \frac{1}{\rho\alpha}. \quad (24)$$

It follows that the conditioned probability of false alarm is given by

$$P_{f|\rho} = e^{-\rho\alpha\eta_T}. \quad (25)$$

The average probability of false alarm is then computed from

$$P_f = \int_0^1 P_{f|\rho} f_\rho(\rho) d\rho \quad (26)$$

where $f_\rho(\rho)$ is given by (12) for the SMI method, and by (14) for the eigenanalysis method. The conditioned output power under \mathbf{H}_1 is given by,

$$\bar{\eta}_1 = \sigma_s^2 + \frac{1}{\rho\alpha} \quad (27)$$

and the conditional probability of detection is

$$P_{d|\rho} = \exp\left(\frac{\eta_T}{\sigma_s^2 + 1/\rho\alpha}\right). \quad (28)$$

The average probability of detection is then expressed:

$$P_d = \int_0^1 P_{d|\rho} f_\rho(\rho) d\rho. \quad (29)$$

These expressions are used later to generate the theoretical probability of detection curves for each of the methods.

B. Robustness

It is well known that the performance of adaptive arrays is affected by calibration errors. Analysis of the Mountain-Top data reported in Section IV reveals target cancellation due to the mismatch between the true received signal vector and the steering vector used in calculating the weights. Also noted in Section IV is the fact that the target cancellation is more pronounced for the SMI than for the eigenanalysis method. This observation motivates the analysis in this section.

Target cancellation occurs when there are calibration errors and the target signal is present during training (estimation of the noise covariance matrix). Since the steering vector is mismatched to the signal vector, the target is interpreted as an interference and the array proceeds to cancel it. To isolate signal cancellation from noise covariance matrix estimation effects, we assume that the true covariance matrix is known. In fact, this assumption accurately represents the case when the weight vector is applied to the data it was derived from.

Additionally, we make the following simplifying assumptions for analytical tractability.

- 1) Processing is carried out only in the spatial domain.
- 2) Calibration errors are limited to the angle of the steering vector. Thus, the target and the presumed steering vector are represented by vectors of the type
$$\mathbf{s}(\theta) = \frac{1}{\sqrt{N}} [1, e^{j\theta}, \dots, e^{j(N-1)\theta}]^T.$$
- 3) There is a single interference represented by the vector \mathbf{s}_i .
- 4) The interference vector is orthogonal to the true target vector, $\mathbf{s}_i^H \mathbf{s} = 0$.

The perturbation model presented above represents the case when the steering vector sweeping an angular sector searching for targets is pointing off-target. A method sensitive to such errors would require a dense search pattern. However, it should be noted that this model is a simplification which does not cover angle errors randomly distributed over the array. These errors lead to waveform distortions rather than an angle error. Thus the simple model used here provides some, if limited, indication of the robustness of the eigencanceler. The Mountain-Top data analysis presented in the next section lends further support to the robustness claims.

The analysis is shown to be invariant to a scaling constant, hence we define the normalized covariance matrix,

$$\mathbf{R} = \mathbf{I} + \bar{\sigma}_s^2 \mathbf{s} \mathbf{s}^H + \bar{\sigma}_i^2 \mathbf{s}_i \mathbf{s}_i^H \quad (30)$$

where $\bar{\sigma}_s^2 = \text{SNR}$ and $\bar{\sigma}_i^2 = \text{INR}$ (interference-to-noise ratio). Performance is investigated through the gain term

$$G = \frac{|\mathbf{w}^H \mathbf{s}|^2}{\mathbf{w}^H \mathbf{R}_i \mathbf{w}} \quad (31)$$

where \mathbf{R}_i is the noise-plus-interference covariance matrix, $\mathbf{R}_i = \mathbf{I} + \bar{\sigma}_i^2 \mathbf{s}_i \mathbf{s}_i^H$. This gain is the ratio of the array output SNR to the input SNR. In the ideal case, when there are no calibration errors, and due to the orthogonality assumed between the interference and the target, it is readily shown that $G = 1$. Consequently, in the presence of calibration errors $0 \leq G \leq 1$. The goal is to characterize G for the SMI and eigenanalysis methods. The SMI weight vector is given by

$$\mathbf{w} = \mathbf{R}^{-1} \tilde{\mathbf{s}} \quad (32)$$

where $\tilde{\mathbf{s}}$ is the presumed steering vector. The eigencanceler weight vector is given by

$$\mathbf{w} = (\mathbf{I} - \mathbf{s}_i \mathbf{s}_i^H) \tilde{\mathbf{s}}. \quad (33)$$

The gain G for each of the methods is computed in the Appendix. For the SMI it is found:

$$G_0 = \frac{|\rho_1|^2 (1 - \gamma_s)^2}{1 - \gamma_s (2 - \gamma_s) |\rho_1|^2 - \gamma_i (2 - \gamma_i) |\rho_2|^2} \quad (34)$$

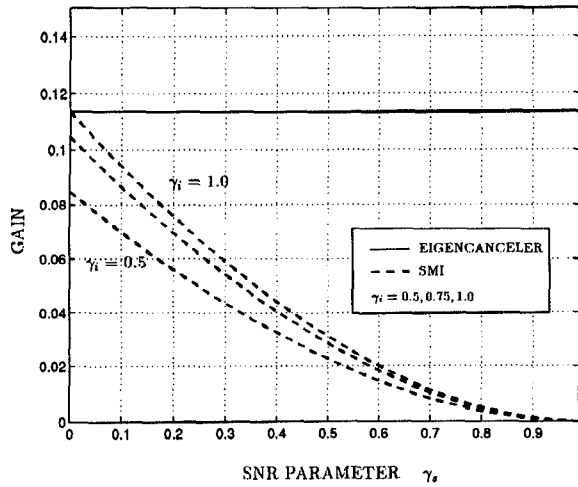


Fig. 2. Signal cancellation effects: G_e , G_0 versus γ_s with γ_i as parameter.

where $\rho_1 = \tilde{s}^H s$, $\rho_2 = \tilde{s}^H s_i$, $\gamma_s = \text{SNR}/(1 + \text{SNR})$, and $\gamma_i = \text{INR}/(1 + \text{INR})$. Note that $0 \leq \gamma_s, \gamma_i \leq 1$. As observed by other authors through similar analysis, G_0 degrades as SNR increases. In the extreme case, $\text{SNR} = \infty$ ($\gamma_s = 1$), and $G_0 = 0$. The other extreme is $G_0 = |\rho_1|^2/(1 - |\rho_2|^2)$, obtained for $\gamma_s = 0$ and $\gamma_i = 1$. The gain term of the eigencanceler is computed in the Appendix and is given by

$$G_e = \frac{|\rho_1|^2}{1 - |\rho_2|^2}. \quad (35)$$

From (34) and (35) it is observed that $G_0 \leq G_e$, with the equality for $\gamma_s = 0$ and $\gamma_i = 1$. Consequently, the eigenanalysis method is less affected by angle calibration errors than the SMI method. This is illustrated in Fig. 2, where G_e and G_0 are plotted for a 14-element array, several values of the SNR factor γ_s , an error angle of $\pi/10$ rad, and an angle of $4\pi/10$ between the presumed steering vector and the interference.

C. Numerical Results

In this subsection, theoretical probability of detection curves are generated for each of the methods, and are compared with simulation. The array has eight elements and four tap delays at each channel. The signal environment consists of clutter distributed in an angular sector. The clutter is distributed between 20 deg and 40 deg. The total input CNR of the distributed clutter equals 15 dB. The look direction steering vector points to 50 deg and 0.5 normalized Doppler frequency. Equation (29), together with (14) and (12), provides the means to analyze the detection performance numerically. Theory and simulations are compared in Figs. 3 and 4. The densities of the conditioned SNR for the eigenanalysis and SMI methods, for $K = 2\nu K$ samples, and as given in (14) and (12), are shown in the lower

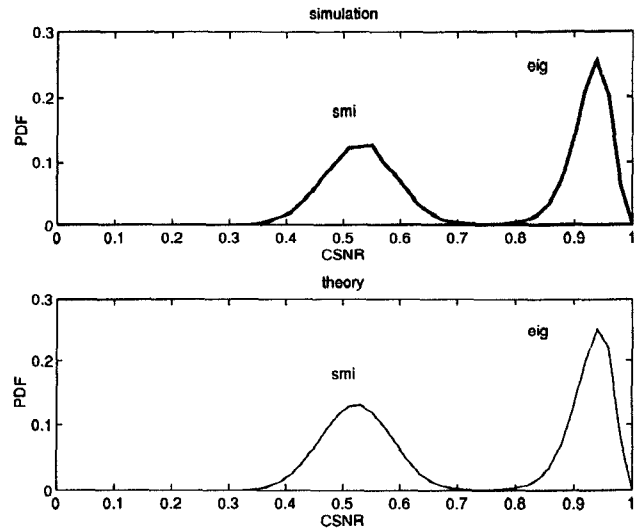


Fig. 3. Probability density of CSNR. Top: simulations. Bottom: theoretical.

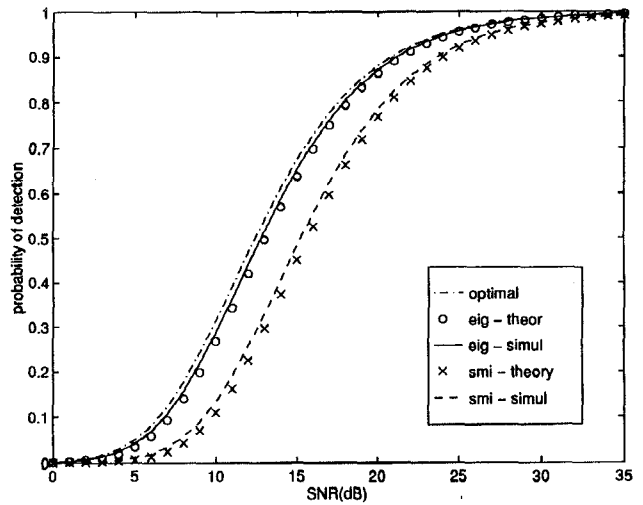


Fig. 4. Probability of detection from theory and simulations.

part of Fig. 3. The eigencanceler was computed using $r = 6$ principal eigenvalues. The upper part of Fig. 3 consists of histograms developed from 10,000 simulation runs. A good fit is observed between the theoretical and the simulation curves. Fig. 4 plots the probability of detection for the various methods, i.e., the average probability of detection versus the input SNR. The detection threshold η_T is found from the solution to (26) when the average probability of false alarm is set to 10^{-5} . The probability of detection is computed using (29). The curve labeled “opt” is the optimal case obtained from (23). The probability of detection curves also show a good fit between theory and simulations.

IV. MOUNTAIN-TOP DATA ANALYSIS

The Mountain-Top program is an Advanced Research Projects Agency (ARPA) sponsored effort

to collect data to support the definition of next generation airborne surveillance radars. The radar measurements are carried out from mountain tops, but radar motion is emulated through a method developed by Lincoln Laboratory [21]. The sensor consists of 14 elements and the data is organized in CPIs of 16 pulses. For the data analyzed here, the clutter was located mainly around 245 deg azimuth and at 156 Hz. A synthetic target was introduced in the data at 154 km, 156 Hz, and 275 deg. Note that the clutter and target have the same Doppler frequency, hence separation is possible only in the spatial domain. Spatial adaptive processing is carried out following bandpass filtering at 156 Hz. Borrowing terminology used in [22], this processing is referred to as post-Doppler. The weight vector length was normalized to one in all plots.

Fig. 5 shows the output of the eigencanceler/SMI at the range cells for which data is available. The output power is measured relative to the skynoise power level, which was computed from separate files in the dataset. The covariance matrix was estimated from 25 samples collected in the 147–150 km range. The weight vector of the eigencanceler was computed utilizing four principal eigenvalues. The output of the nonadaptive beamformer is also shown for reference. With the nonadaptive beamformer the clutter is high and the target is not visible. Both adaptive methods are seen to extract the target from the clutter, the eigenanalysis-based method, however, exhibits a better signal-to-clutter ratio in the vicinity of the target. Note also the deep cancellation by the SMI in the training region of 147–150 km. To generate Fig. 6, the steering vector was scanned over the angular range of the abscissa. The covariance matrix was estimated as in Fig. 5. Thus, the figure shows the echo magnitude at the target range cell and for beamforming at various angles. The gain is measured with respect to the output of the eigencanceler when the beamformer points in the actual target direction (target located at 275 deg). This plot emulates the radar angle scan. The nonadaptive beamformer return closely matches the clutter pattern (clutter is located around 245 deg). The SMI adapted pattern does not peak in the direction of the target, hence a scan using this method will likely miss the target. Conversely, the eigenanalysis-method pattern clearly peaks in the target direction.

Effects of calibration errors can be assessed when the array is trained using the data around, and including, the target region. Since weight vectors are applied back to the data they were derived from, we are not concerned with the statistical fluctuations in the estimate of the covariance matrix. However, since the signal was present during training, cancellation will occur to the extent that the presumed steering vector is different from the true target vector. The target signal is present in only a limited number of

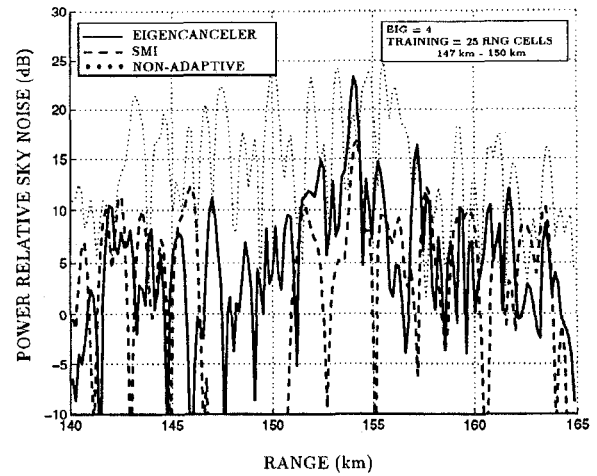


Fig. 5. Output power relative to skynoise versus range. Training without target present.

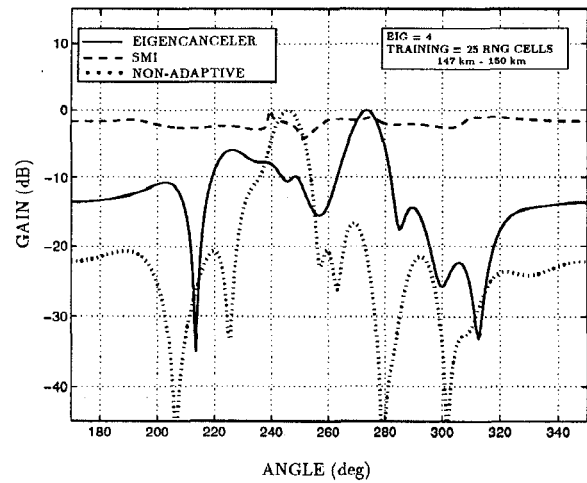


Fig. 6. Signal magnitude as function of pointing direction.

range cells. The covariance matrix can be expressed

$$\mathbf{R} = \frac{1}{K} \sum_{k=1}^K \mathbf{x}_k \mathbf{x}_k^H + \frac{1}{K} \sum_{m=1}^M |a_m|^2 \mathbf{s} \mathbf{s}^H \quad (36)$$

where M is the number of range cells for which there is a significant target return and a_m are the target complex amplitudes. Our discussion is concerned with the effect of increasing K (the training region) while keeping M fixed. Since M is fixed, the signal power (contributions collected over the M range cells containing the target) decreases with respect to the power of the K range cells used in the training. This has the effect of decreasing SNR as the training region (i.e., K) is increased. A measure of signal cancellation is provided by measuring the factor r , defined as the ratio of the target peak level for given training to the peak level when training is done over all 300 range cells. Target cancellation is measured by $1 - r$ and is plotted in Fig. 7. Note that increasing the number of training samples is tantamount to decreasing the SNR.

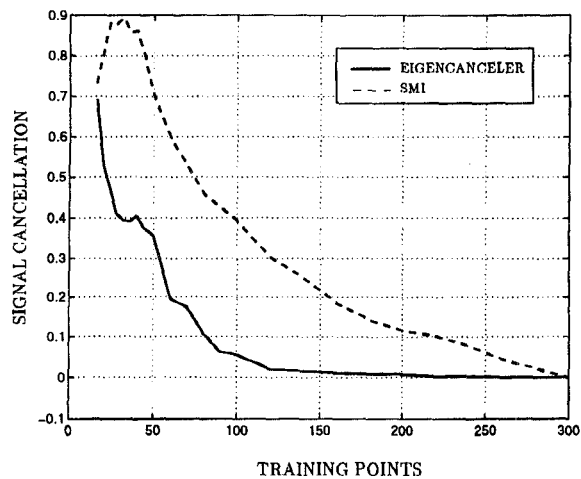


Fig. 7. Signal cancellation as function of decreasing SNR.

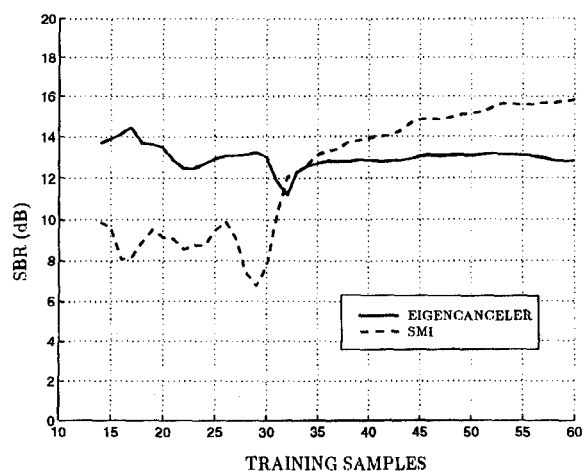


Fig. 8. SBR versus number of training samples.

Clearly, the eigenanalysis method exhibits lower signal cancellation than the SMI.

When training is carried out outside the target region (as in Fig. 5), the performance is indicative of the effects of covariance matrix estimation. Fig. 8 plots the signal-to-background ratio (SBR) averaged over three CPIs, and as a function of the number of training samples. The background signal level was measured from 50 range cells around the target region, and the target was measured at peak value. The plot exhibits the expected characteristics of the two methods: when the number of samples is low, the eigenanalysis method clearly has the advantage. As the number of samples increases, the performance of the SMI method improves.

Fig. 9 shows the effect of the number of principal eigenvectors used in deriving the weight vector of the eigencanceler. The training was the same as in Fig. 5 and the background was measured like in Fig. 8. The SBR was averaged over three CPIs.

In an actual application, STAP needs to be performed in real-time. The weight vector is

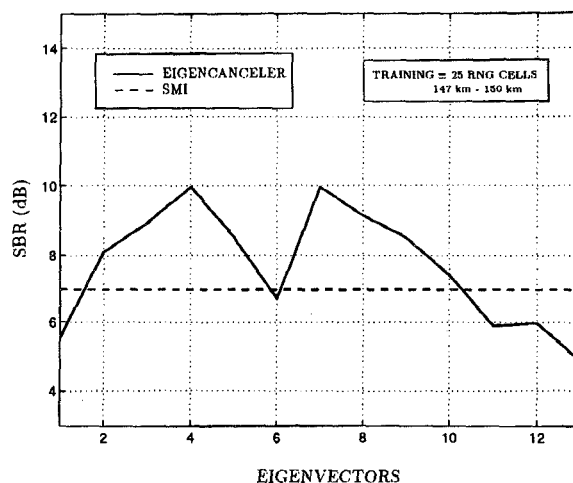


Fig. 9. SBR as function of number of eigenvectors used.

computed from the sample covariance matrix estimated over a CPI. As shown in the theoretical analysis and illustrated by the data analysis, SMI may result in target cancellation if the target is included in the training data. Thus, SMI requires training strategies such that the cell under test is excluded from the data prior to the weight vector computation. The eigencanceler was shown to be robust to target cancellation effects. Thus application of the eigencanceler may entail simple training strategies, possibly the use of the same weight vector for all range cells, which may facilitate real-time implementation.

V. CONCLUSIONS

In this paper we studied eigenanalysis-based detection for airborne surveillance radars and compared the performance with that of the SMI method. Analytical expressions for the receiver operating characteristics were obtained based on the asymptotic expansion of the distribution of the principal components of the covariance matrix and were corroborated by simulations. The results clearly indicate the higher convergence rate of the eigenanalysis method. Further confirmation was obtained from analyzing Mountain-Top data. Expressions were developed to characterize the robustness with respect to the pointing error. This model is a simplification of the more general case of random angle errors. While the conclusions drawn from this analysis are limited to this simple, mathematically tractable case, the robustness of the eigenanalysis method was also demonstrated by analysis of the Mountain-Top dataset, which of course incorporates errors associated with a real system operation. These results may further the development of robust, efficient, STAP algorithms, supported by simple training strategies which do not require the exclusion of the cell under test from the training set.

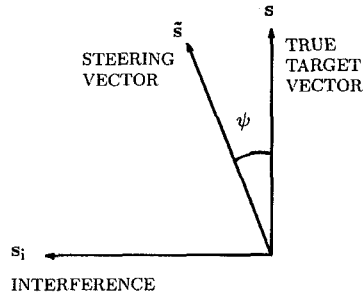


Fig. 10. Geometry for robustness analysis.

APPENDIX. DERIVATIONS OF (34) AND (35)

This Appendix provides the proof to (34) and (35). From (30), and through two consecutive applications of the matrix inversion lemma, one obtains a closed-form expression for the inverse of the normalized covariance matrix:

$$\mathbf{R}^{-1} = \mathbf{I} - \gamma_s \mathbf{s} \mathbf{s}^H - \gamma_i \mathbf{s}_i \mathbf{s}_i^H$$

where γ_s and γ_i are defined in Section III. The gain to be calculated is defined in (31). Consider the numerator and denominator of G , for the SMI weight vector in (32):

$$\begin{aligned} \text{NUM1} &= |\tilde{\mathbf{s}}^H \mathbf{R}^{-1} \mathbf{s}|^2 \\ &= |\rho_1|^2 (1 - \gamma_s)^2 \end{aligned}$$

where the inner product between the presumed and true steering vectors is $|\rho_1|^2 = |\tilde{\mathbf{s}}^H \mathbf{s}|^2 = (1/N)(\sin^2 N\psi / \sin^2 \psi)$, where ψ is the angle between the vectors as shown in Fig. 10, and it is assumed that $\mathbf{s}^H \mathbf{s}_i = 0$. The denominator of the gain term is given by

$$\begin{aligned} \text{DEN1} &= \tilde{\mathbf{s}}^H \mathbf{R}^{-1} \mathbf{R}_i \mathbf{R}^{-1} \tilde{\mathbf{s}} \\ &= \tilde{\mathbf{s}}^H (\mathbf{I} - \gamma_s \mathbf{s} \mathbf{s}^H - \gamma_i \mathbf{s}_i \mathbf{s}_i^H)^{-1} \tilde{\mathbf{s}} \\ &= \tilde{\mathbf{s}}^H [\mathbf{I} - \gamma_s (2 - \gamma_s) \mathbf{s} \mathbf{s}^H - \gamma_i (2 - \gamma_i) \mathbf{s}_i \mathbf{s}_i^H] \tilde{\mathbf{s}} \end{aligned}$$

where $\mathbf{R}_i = \mathbf{I} + \sigma_i^2 \mathbf{s}_i \mathbf{s}_i^H$. Defining $|\rho_2|^2 = |\tilde{\mathbf{s}}^H \mathbf{s}_i|^2$ we obtain

$$\text{DEN1} = 1 - \gamma_s (2 - \gamma_s) |\rho_1|^2 - \gamma_i (2 - \gamma_i) |\rho_2|^2$$

and relation (34) follows.

For the eigencanceler from (33) we have

$$\begin{aligned} \text{NUM2} &= |\tilde{\mathbf{s}}^H (\mathbf{I} - \mathbf{s}_i \mathbf{s}_i^H) \mathbf{s}|^2 \\ &= |\rho_1|^2 \end{aligned}$$

and

$$\begin{aligned} \text{DEN2} &= \tilde{\mathbf{s}}^H (\mathbf{I} - \mathbf{s}_i \mathbf{s}_i^H) \mathbf{R}_i (\mathbf{I} - \mathbf{s}_i \mathbf{s}_i^H) \tilde{\mathbf{s}} \\ &= 1 - |\rho_2|^2 \end{aligned}$$

and relation (35) follows.

REFERENCES

- [1] Brennan, L. E., and Reed, I. S. (1973) Theory of adaptive radar. *IEEE Transactions on Aerospace and Electronic Systems*, **AES-9** (Mar. 1973), 237–252.
- [2] Reed, I. S., et al. (1974) Rapid convergence rates in adaptive arrays. *IEEE Transactions on Aerospace and Electronic Systems*, **AES-10** (Nov. 1974), 853–863.
- [3] Boroson, D. M. (1980) Sample size considerations for adaptive arrays. *IEEE Transactions on Aerospace and Electronic Systems*, **AES-16** (July 1980), 446–451.
- [4] Hanumara, R. C. (1986) An alternate derivation of the distribution of the conditioned signal-to-noise ratio. *IEEE Transactions on Antennas Propagation*, **AP-34** (Mar. 1986), 463–464.
- [5] Khatri, C. G. (1987) Effects of estimated noise covariance matrix in optimal signal detection. *IEEE Transactions on Acoustics, Speech, and Signal Processing*, **ASSP-35** (May 1987), 671–679.
- [6] Kelly, E. J. (1986) An adaptive detection algorithm. *IEEE Transactions on Aerospace and Electronic Systems*, **AES-22** (Mar. 1986), 115–127.
- [7] Cox, H. (1973) Resolving power and sensitivity to mismatch of optimum array processors. *Journal of the Acoustical Society of America*, **54** (1973), 771–785.
- [8] Jablon, N. K. (1986) Adaptive beamforming with the generalized sidelobe canceller in the presence of array imperfections. *IEEE Transactions on Antennas Propagation*, **AP-34** (Aug. 1986), 996–1012.
- [9] Er, M. H., and Cantoni, A. (1985) An alternative formulation for an optimum beamformer with robustness capability. *Proceedings of the IEEE*, (Oct. 1985), 447–460.
- [10] Feldman, D., and Griffith, L. J. (1994) A projection approach for robust adaptive beamforming. *IEEE Transactions on Signal Processing*, **42** (Apr. 1994), 867–876.
- [11] Cai, L., and Wang, H. (1991) Performance comparisons of modified SMI and GLR algorithms. *IEEE Transactions on Aerospace and Electronic Systems*, **27** (May 1991), 487–491.
- [12] Nitzberg, R. (1992) *Adaptive Signal Processing for Radar*. Norwood, MA: Artech House, 1992.
- [13] Haimovich, A. M. (1994) The eigencanceler: A new space-time interference canceler. In *Proceedings of the 1994 IEEE National Radar Conference*, Atlanta, GA, 1994, 194–198.
- [14] Haimovich, A. M. (1996) The eigencanceler: Adaptive radar by eigenanalysis methods. *IEEE Transactions on Aerospace and Electronic Systems* (Apr. 1996), 532–542.
- [15] Kirsteins, I. P., and Tufts, D. W. (1994) Adaptive detection using low rank approximation to a data matrix. *IEEE Transactions on Aerospace and Electronic Systems*, **30** (Jan. 1994), 55–67.

- [16] Monzingo, R., and Miller, T. (1980)
An Introduction to Adaptive Arrays.
New York: Wiley, 1980.
- [17] Haimovich, A. M., and Bar-Ness, Y. (1991)
An eigenanalysis interference canceler.
IEEE Transactions on Acoustics, Speech, and Signal Processing, **39** (Jan. 1991), 76–84.
- [18] Kirsteins, I. P., and Tufts, D. W. (1991)
Rapidly adaptive nulling of interference.
In M. Bouvet and G. Bienvenu (Eds.), *High Resolution Methods in Underwater Acoustics*.
New York: Springer, 1991, ch. 6, 220–249.
- [19] Haimovich, A. M. (1995)
Asymptotic distribution of the conditioned signal-to-noise ratio in an eigenanalysis-based adaptive array.
IEEE Transactions on Aerospace and Electronic Systems, **33**, 3 (July 1997), 988–997.
- [20] Klemm, R. (1983)
Adaptive clutter suppression for airborne phased array radars.
Proceedings of the IEE, **130**, Pts. F and H (Feb. 1983), 125–132.
- [21] Titi, G. W. (1994)
An overview of the ARPA mountaintop program.
In *Proceedings of the 1994 Adaptive Antenna Systems Symposium*, Melville, NY, Nov. 1994, 53–59.
- [22] Marshall, D. F. (1994)
A two step adaptive interference nulling algorithm for use with airborne sensor arrays.
In *Proceedings Seventh SP Workshop on Statistical Signal and Array Processing*, Quebec City, Canada, June 26–29, 1994, 301–304.



Alexander Haimovich received the B.S. degree from the Technion Institute of Technology, Israel, the M.S. degree from Drexel University, Philadelphia, PA, both in electrical engineering, and the Ph.D. degree in systems from the University of Pennsylvania, Philadelphia, in 1977, 1982, and 1989, respectively.

He is currently an Associate Professor of Electrical Engineering at the New Jersey Institute of Technology. His professional record includes positions at JJM Systems, Ivyland, PA as Chief Scientist from 1990 to 1992, and at American Electronic Laboratories, Lansdale, PA as Senior Staff Consultant from 1989 to 1990. Prior to this Dr. Haimovich was a Lecturer at the New Jersey Institute of Technology from 1987 to 1989 and a Senior Engineer at American Electronic Laboratories from 1983 to 1987. His research interests include adaptive arrays with applications to radar and mobile communications signal processing and signal separation in multiuser communication systems.



Murat Berin was born in Istanbul, Turkey, on May 22, 1970. He received the B.S. and M.S. degrees in 1994 and 1996 from the New Jersey Institute of Technology (NJIT), in electrical engineering.

From 1994 to 1996, he was a research assistant in Center for Communications and Signal Processing Research, NJIT, involved in a joint project with the U.S. Air Force. He is currently employed by Expert Wireless Solutions Inc., Fort Lee, NJ.